First experiments on diffraction-enhanced imaging at LNLS

C. Giles,[a,b]* M. G. Hönnicke,[c] R. T. Lopes,[d] H. S. Rocha,[d] O. D. Gonçalves,[e] I. Mazzaro[c] and C. Cusatis[c]

[a]Instituto de Física, Universidade Estadual de Campinas, SP, Brazil, [b]Laboratório Nacional de Luz Síncrotron, Campinas, SP, Brazil, [c]Departamento de Física, Universidade Federal do Paraná, Curitiba, PR, Brazil, [d]COPPE, Universidade Federal do Rio de Janeiro, Rio de Janeiro, RJ, Brazil, and [e]Instituto de Física, Universidade Federal do Rio de Janeiro, Rio de Janeiro, RJ, Brazil. E-mail: giles@ifi.unicamp.br

Diffraction-enhanced images have been obtained using two silicon crystals in a non-dispersive set-up at the XRD2 beamline at the Brazilian Synchrotron Light Laboratory (LNLS). A first asymmetrically cut silicon crystal using the (333) reflection vertically expanded the monochromated beam from 1 mm to 20 mm allowing the imaging of the whole sample without movements. A symmetrically cut Si(333) second crystal was used as a Bragg analyzer. Images of biological samples including human tissue were recorded using a direct-conversion CCD detector resulting in enhancement of the contrast compared with absorption-contrast images.

Keywords: X-ray imaging; phase-contrast imaging; diffraction-enhanced imaging; X-ray optics.

1. Introduction

Traditional X-ray imaging is based on the absorption contrast of different parts of an object. Progress in this field has been made on the improvement of detectors such as image plates, flat-panel detectors, CCD cameras *etc.*, and developments on source and optical elements. Enhanced imaging quality has been recently achieved by exploring the real component δ of the refractive index ($n = 1 - \delta - i\beta$) instead of the imaginary component $i\beta$ that is responsible for absorption (Ingal & Beliaevskaya, 1995; Snigirev *et al.*, 1995; Wilkins *et al.*, 1996). Different optical arrangements and techniques, generally termed as phase-contrast radiography (PCR) or diffraction-enhanced imaging (DEI) (Chapman *et al.*, 1997), are being used to increase the density of information carried by the X-ray beam that passes through the object and reaches the detector. For PCR, as in the case when an X-ray interferometer is used, beam coherence is the fundamental factor (Ando *et al.*, 2001). However, angular rejection of photons scattered at small angles or deviated by refraction (Ando *et al.*, 2001), which are described by the real component of the refractive index, can be used by optical methods to increase the contrast. Projection radiography simply using a point source (Wilkins *et al.*, 1996), X-ray holography using a coherent or partially coherent source (Tegze *et al.*, 2000) and non-dispersive double-crystal radiography (Davis *et al.*, 1995; Förster *et al.*, 1980), together with X-ray interferometry (Ando & Hosoya, 1972), are some of the techniques used to obtain contrast originating from the real component of the refractive index. Applications of this technique are spreading as the experiments are being intensively developed (Stevenson *et al.*, 2003).

First experiments on DEI have begun at the Brazilian Synchrotron Light Laboratory (LNLS) and are reported here. The experimental set-up will be described in detail; DEI obtained with synchrotron radiation will be shown and compared with absorption radiography of the same samples. Conclusions and perspectives will be drawn.

2. Experiment

Synchrotron light properties are very suitable for obtaining enhanced radiographic imaging (Snigirev *et al.*, 1995; Zhong *et al.*, 2000; Westneat *et al.*, 2003; Stevenson *et al.*, 2003). First experiments of DEI have been optimized at the XRD2 high-resolution X-ray diffraction beamline (Giles *et al.*, 2003). A double-crystal Si(111) pre-monochromator, upstream of the beamline, was used to select a small energy bandwidth ($\Delta\lambda/\lambda = 3 \times 10^{-4}$) at 8 keV. A non-dispersive set-up (Ingal & Beliaevskaya, 1995) was used with an asymmetrically cut ($b = -0.05$) Si(333) first crystal to expand the beam and a symmetrically cut Si(333) second crystal as a Bragg analyzer (Fig. 1). The two-crystal set-up had mechanical and thermal stability assured by the use of a robust double-axis diffractometer made of one solid piece of melted iron and positioned in the vertical scattering geometry. The distance between the two axes, 200 mm, allowed convenient sample positioning. A direct-conversion water-cooled CCD camera of 1242 pixels × 1152 pixels, each 25 μm × 25 μm, positioned at 200 mm from the analyzer crystal, was used as a two-dimensional detector. With this set-up it was possible to obtain bright and dark field images by changing the angular position of the Bragg analyzer crystal by some tens of μrad around the maximum of the rocking curve. The acquisition time varied with the transmitted signal through the sample and with the angular position of the Bragg analyzer crystal, from a few seconds to several minutes per image. Images obtained with this set-up were compared with conventional absorption radiographs taken using the same samples with a conventional laboratory source.

The phase contrast becomes very useful at higher energies and very suitable for enhanced imaging of low-density objects.

3. Results

To demonstrate DEI effects, images were taken of a tree leaf at different angular positions of the Bragg analyzer crystal. Fig. 2(*a*) was recorded with the analyzer near the peak position showing dark contrast at the stem, indicated by the arrow. Images of the tree leaf

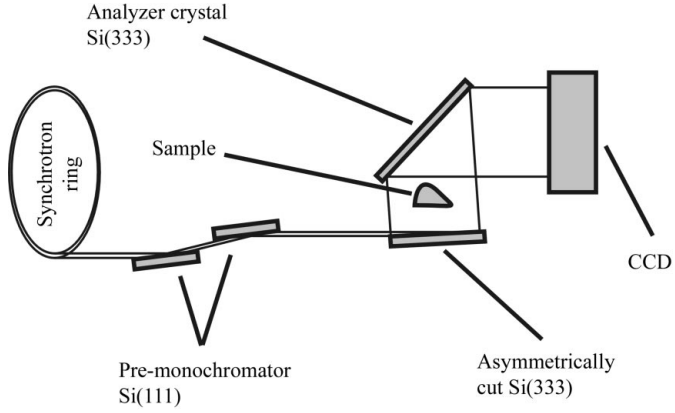

Figure 1
DEI set-up at the XRD2 beamline. A non-dispersive set-up prepares the X-ray beam to obtain enhanced quality transmission images of different specimens. The first crystal is asymmetrically cut ($b = -0.05$) to expand the beam. At different angular positions of the Bragg analyzer (by varying the diffraction angle) it is possible to obtain dark and bright field contrast recorded by a CCD detector.

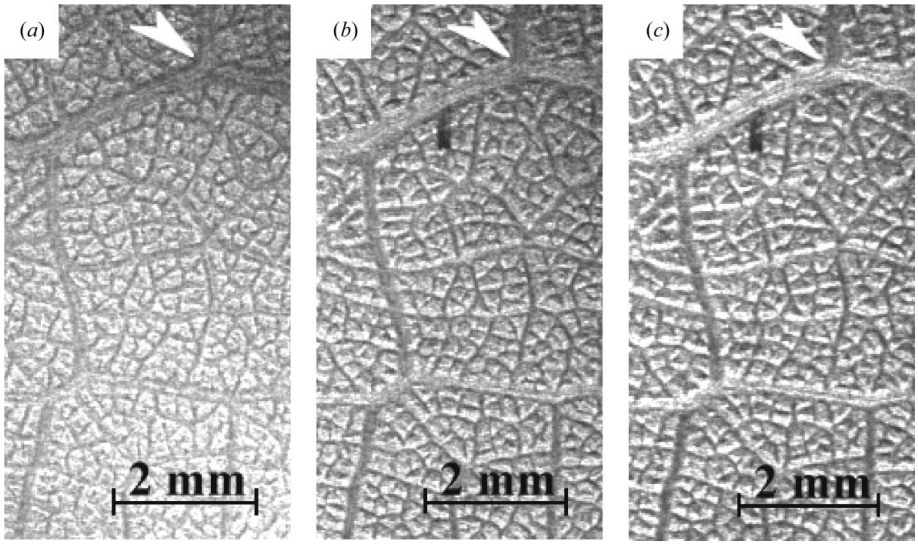

Figure 2
DEI of a tree leaf at different angular positions of the analyzer crystal. (*a*) Near to the analyzer peak position. (*b*) and (*c*) At different angular positions further away from the peak positions (see Fig. 3). Contrast inversion (dark to bright) at some features of the leaf stem (indicated by the arrow), only possible with phase-contrast techniques, is demonstrated. Exposure times: (*a*) 2 min; (*b*) and (*c*) 6 min.

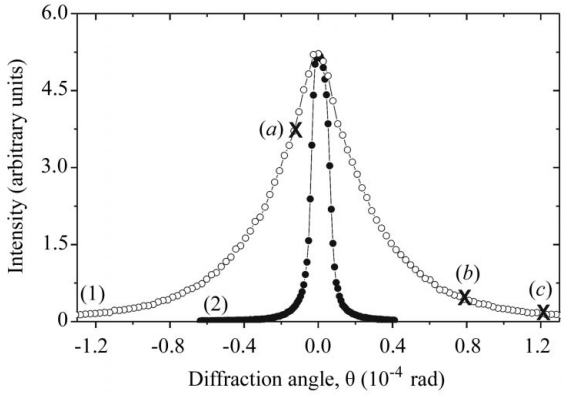

Figure 3
(1): Rocking curve of the crystal analyzer Si(333) after transmission through the tree leaf. Crosses indicate the angular positions of the analyzer crystal for the images of Fig. 2 (*a*)–2(*c*). (2): Rocking curve of the crystal analyzer without a sample. The rocking-curve width is enlarged by the transmission of the beam through the specimen positioned between this non-dispersive crystal set-up.

with increasing angular distance from the peak position creates an inversion of the DEI contrast from dark to bright in the entire image and in particular at the stem indicated by the arrow (Figs. 2*a*–2*c*). A schematic rocking curve of the Si(333) analyzer crystal with the beam passing through the sample is shown in Fig. 3. The angular positions where the tree-leaf images of Fig. 2 were taken are indicated by crosses. Images far from the peak position required more integration time to account for the intensity decrease out of the analyzer peak position. The demonstrated tunability from dark to bright contrast is not possible in absorption-contrast imaging and is characteristic of the phase-contrast techniques.

DEI is also being used to improve the distinction between normal and abnormal human tissue. This may be useful in the case of the identification of microcalcifications (Arfelli *et al.*, 2000) and surface spiculations that could be correlated with histopathologic information to detect early stages of tumor tissue and its extension into the surrounding tissue. Figs. 4 and 5 show examples of DEI with *in vitro* tumorous tissue. A sectional image of a formalin-fixed human uterus cancer specimen is shown in Fig. 4(*a*). An absorption-contrast image (Fig. 4*b*) and diffraction-enhanced image (Fig. 4*c*) of a small region containing tumorous tissue indicated by the arrow are shown for comparison. Increased contrast details present in the diffraction-enhanced image are indications of the potential application of this technique for detection of lesion details for early diagnosis and characterization of histopathologic tissue. A lung specimen with tubercular regions is shown in Fig. 5. A sectional image with arrows indicating the internal structure of a tuberculoma is shown in Fig. 5(*a*) and is compared with the absorption-contrast (Fig. 5*b*) and DEI (Fig. 5*c*) images. The tubercular structures are clearly visible in the DEI image compared with the absorption-contrast image.

Another example is shown in Fig. 6, in a study of tooth radiography. A 0.5 mm-thick canine sectional specimen was used for absorption-contrast imaging (Fig. 6*a*) and DEI (Fig. 6*b*). The enamel and dentine interface is clearly visible in the DEI image.

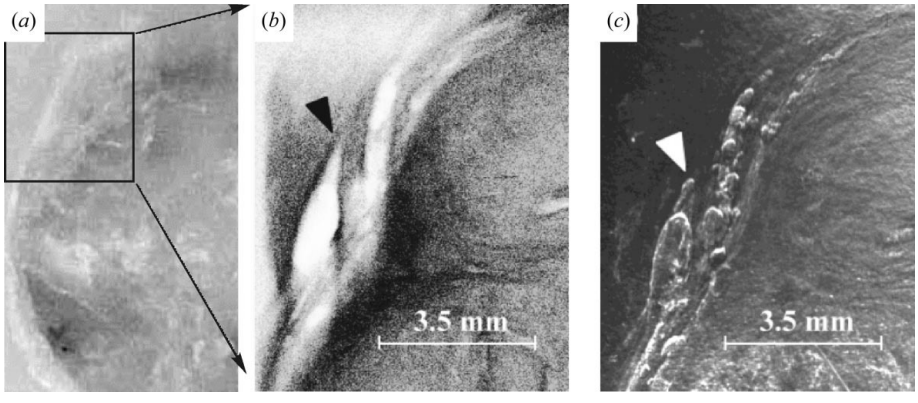

Figure 4
(*a*) Image of a sectional *in vitro* human uterus specimen with visible light. The region selected was observed using (*b*) absorption radiography and (*c*) DEI. Note that the features in (*c*) shown by arrows correspond to details related to tumorous tissue presenting resolution and contrast details not seen in the absorption radiograph. Exposure times: (*b*) 1 min and (*c*) 15 min.

4. Conclusions and perspectives

A DEI set-up has been implemented at the high-resolution X-ray diffraction beamline XRD2 at the LNLS. First experiments using an asymmetrically cut Si(333) and a symmetrically cut Si(333) crystal as a Bragg analyzer allowed DEI of biological specimens. Bright and dark field enhanced contrast of boundaries between media of different density was shown. One possible application of DEI radiography is the advanced observation of microcalcifications in mammographic images which can be one of the first signs of breast cancer and is not straightforwardly detected by conventional X-ray imaging.

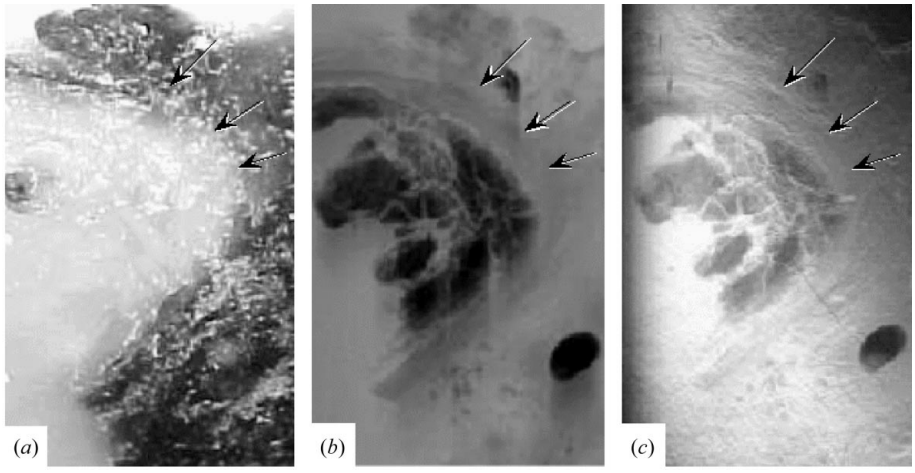

Figure 5
(*a*) Image of a sectional *in vitro* human lung specimen. Features indicated by arrows are structures of tubercular tissue. (*b*) Absorption-contrast image and (*c*) diffraction-enhanced image of the same region. The DEI image improved the visualization of the pathological structures in this specimen. Exposure times: (*b*) 1 min and (*c*) 5 min.

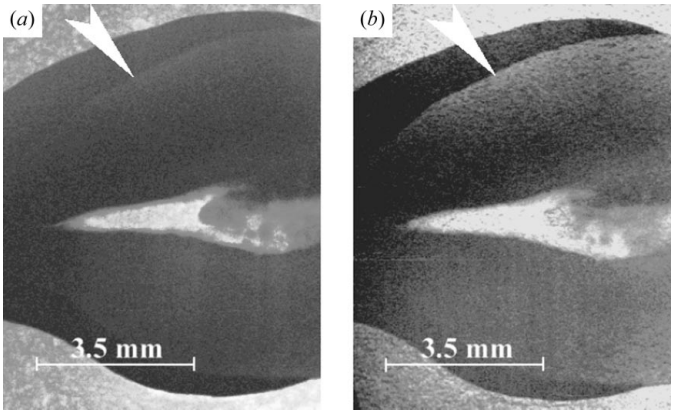

Figure 6
Images of a 0.5 mm-thick *in vitro* canine human tooth sectional specimen obtained by (*a*) absorption-contrast imaging and (*b*) DEI. The boundary between the enamel and dentine (indicated by the arrow) is clearly enhanced using the DEI technique. Exposure times: (*a*) 3 min and (*b*) 10 min.

This work is part of a recently created collaborative network between our research institutions (UFRJ, UNICAMP, LNLS and UFPR). Further experiments using synchrotron radiation at higher energies as well as alternative set-ups for DEI using synchrotron radiation and conventional sources will be performed in the near future.

This work was partially supported by Conselho Nacional de Desenvolvimento Científico e Tecnológico (CNPq), Fundação de Amparo à Pesquisa do Estado de São Paulo (FAPESP contract 96/05586-6) and Programa de Apoio à Núcleos de Excelência (PRONEX).

References

Ando, M. & Hosoya, S. (1972). *Proceedings of the 6th International Conference on X-ray Optics and Microanalysis*, edited by G. Shinoda *et al.*, p. 63. Tokyo: University of Tokyo.
Ando, M., Sugiyama, H., Zhang, X., Hyodo, K., Maksimenko, A. & Pattanasiriwisawa, W. (2001). *Jpn. J. Appl. Phys.* **40**, L298–L301.
Arfelli, F., Bonvicini, V., Bravin, A., Cantatore, G., Castelli, E., Palma, L. D., Di Michiel, M., Fabrizioli, M., Longo, R., Menk, R. H., Olivo, A., Pani, S., Pontoni, D., Poropat, P., Prest, M., Rashevsky, A., Ratti, M., Rigon, L., Tromba, G., Vacchi, A., Vallazza, E. & Zanconati, F. (2000). *Radiology*, **215**, 286–293.
Chapman, D., Thomlinson, W., Johnston, R. E., Washburn, D., Pisano, E., Gmür, N., Zhong, Z., Menk, R., Arfelli, F. & Sayers, D. (1997). *Phys. Med. Biol.* **42**, 2015–2025.
Davis, T. J., Gao, D., Guruyev, T. E., Stevenson, A. W. & Wilkins, S. W. (1995). *Nature (London)*, **373**, 595–598.
Förster, E., Goetz, K. & Zaumsell, P. (1980). *Kryst. Tech.* **15**, 937–945.
Giles, C., Yokaichiya, F., Kycia, S. W., Sampaio, L. C., Ardiles-Saravia, D. C., Franco, M. K. K. & Neuenschwander, R. T. (2003). To be published.
Ingal, V. N. & Beliaevskaya, E. A. (1995). *J. Phys. D*, **28**, 2314–2317.
Snigirev, A., Snigireva, I., Kohn, V., Kuznetsov, S. & Schelokov, I. (1995). *Rev. Sci. Instrum.* **66**, 5486–5492.
Stevenson, A. W., Gureyev, T. E., Paganin, D., Wilkins, S. W., Weitkamp, T., Snigirev, A., Rau, C., Snigireva, I., Youn, H. S., Dolbnya, I. P., Yun, W., Lai, B., Garrett, R. F., Cookson, D. J., Hyodo, K. & Ando, M. (2003). *Nucl. Instrum. Methods Phys. Res. B*, **199**, 427–435.
Tegze, M., Faigel, G., Marchesini, S., Belakhovsky, M. & Ulrich, O. (2000). *Nature (London)*, **407**, 38.
Westneat, M. W., Betz, O., Blob, R. W., Fezzaa, K., Cooper, W. J. & Lee, W. K. (2003). *Science*, **299**, 558–560.
Wilkins, S. W., Gureyev, T. E., Gao, D., Pogany, A. & Stevenson, A. W. (1996). *Nature (London)*, **384**, 335–338.
Zhong, Z., Thomlinson, W., Chapman, D. & Sayers, D. (2000). *Nucl. Instrum. Methods Phys. Res. A*, **450**, 556–567.

 Received 24 May 2003 • Accepted 15 September 2003